

Insights into the Hydrogen-Related Mechanism behind Defect Formation during Light- and Elevated-Temperature-Induced Degradation

Benjamin Hammann,* Lazhar Rachdi, Wolfram Kwapil, Florian Schindler,* and Martin C. Schubert


By investigating the formation of light- and elevated-temperature-induced degradation (LeTID) defects under dark annealing conditions alongside the formation of the boron–hydrogen complex, it is found that both formations are limited by presumably the same reaction. Starting with this observation, two possible mechanisms of LeTID defect formation, a hydrogen-related association and dissociation process, are discussed. Including the current knowledge on hydrogen in silicon as well as on the reverse reaction to the defect formation, the dissociation mechanism seems to be more likely: the LeTID precursor is composed of hydrogen being bound to another complex. During dark annealing, the hydrogen dissociates and binds to its sink, which herein is boron. The remaining complex is recombination active and leads thus to the observed degradation.

1. Introduction

Over many decades, silicon solar cells benefited from hydrogen due to its ability to passivate defects or elicit the regeneration of the boron–oxygen defect.^[1,2] With the discovery of light- and elevated-temperature-induced degradation (LeTID) in 2012,^[3] it was soon assumed that hydrogen plays a key role in causing LeTID, which can result in efficiency losses of up to 10%_{rel}.^[4]

B. Hammann, L. Rachdi, Dr. W. Kwapil, Dr. F. Schindler, Dr. M. C. Schubert
 Department Quality Assurance, Characterization and Simulation
 Fraunhofer Institute for Solar Energy Systems (ISE)
 Heidenhofstraße 2, Freiburg 79110, Germany
 E-mail: benjamin.hammann@ise.fraunhofer.de;
 florian.schindler@ise.fraunhofer.de

Dr. W. Kwapil
 Laboratory for Photovoltaic Energy Conversion
 Department of Sustainable Systems Engineering (INATECH)
 University of Freiburg
 Emmy-Noether-Str. 2, Freiburg 79110, Germany

 The ORCID identification number(s) for the author(s) of this article can be found under <https://doi.org/10.1002/pssr.202000584>.

© 2021 The Authors. physica status solidi (RRL) Rapid Research Letters published by Wiley-VCH GmbH. This is an open access article under the terms of the Creative Commons Attribution-NonCommercial-NoDerivs License, which permits use and distribution in any medium, provided the original work is properly cited, the use is non-commercial and no modifications or adaptations are made.

DOI: 10.1002/pssr.202000584

The LeTID defect (*LD*) itself has been found in different Si materials such as multicrystalline (mc)-Si,^[3] Czochralski-Si,^[5] and float-zone (FZ) Si.^[6,7] The activation or formation of *LD* has been observed under light soaking as well as under dark annealing^[8] but always at elevated temperatures. The behavior can generally be described with a three-state (or, for some specific cases,^[9] with a four-state) model. The first of the three states represents the initial state before degradation, where the recombination-inactive LeTID precursor (*LP*) is present. During degradation, *LP* transforms into the highly recombination-active *LD* (second state). During prolonged treatment, the defect is converted into a recombination-inactive state (third state).

The behavior of hydrogen in silicon has been the object of research for many decades. While the understanding on hydrogen has improved significantly, important physical quantities are still under debate, e.g., the exact diffusivity of different H charge states at different temperatures. A thorough review on the current knowledge can be found in the study by Hamer et al.^[10] In recent years, attempts have been made to understand the role of hydrogen in LeTID by varying external parameters such as sample thickness^[11] or dark annealing/light soaking conditions.^[9] Fung et al. used previously published data on B–H pair concentration to interpret B–H pairs as part of the precursor in their model,^[12] and Chen et al. simulated the changes in monoatomic hydrogen fraction across a p–n junction to understand the movement of hydrogen that can occur during LeTID treatment.^[13] While Schmidt et al. discussed a correlation of the maximum LeTID extent in mc-Si with the B–H pair concentration in FZ-Si,^[14] no deeper link between both quantities was established. In recent years, different models were proposed on how *LP* is created and how *LD* is formed and subsequently annihilated.^[13–15]

In a recent study, we presented a numerical model for the temperature-dependent hydrogen kinetics based on the current knowledge about hydrogen.^[16] We suggested that the LeTID defect formation is a dissociation process with hydrogen dissociating from the LeTID precursor. As the solubility of unbound hydrogen in silicon is very low, significant dissociation—and hence degradation—only occurs if the released hydrogen is bound to other sinks, e.g., boron to form B–H pairs. This implies that the formation kinetics of *LD* and the

hydrogen–sink complex should show a significant amount of correlation. As opposed to previous publications,^[12,14,17] we measure hydrogen-related changes as well as *LD* formation under the same treatment condition and on the same wafers (see Experimental Section). This method allows for a more in-depth analysis of the occurring mechanisms and gives significant insight into the role of hydrogen during LeTID defect formation.

2. Experimental Results

To be able to compare B–H pairs and *LD* formation, both quantities have to be measured on the same wafer (see Experimental Section for details). **Figure 1** shows the change in LeTID defect density extracted from effective lifetime τ_{eff} and the evolution of B–H pair concentration during dark annealing at 160 °C, calculated from Equation (1) and (2) (cf. Experimental Section).

The transformation of *LP* into the recombination-active *LD* leads to the first increase in ΔN_{LD} , as shown in **Figure 1a**. Subsequently, after $\approx 3 \times 10^3$ min, *LD* appears to deactivate, resulting in a decrease in ΔN_{LD} . A second increase in apparent defect concentration is visible after long treatment times ($t > 10^4$ min), which can be attributed to the degradation of surface passivation,^[18] confirmed by a strong increase in the measured surface saturation current density J_{0s} (data not shown). **Figure 1b** shows the evolution of [BH] throughout the experiment. During the firing step, the resistivity slightly increases, reflected in the increase in [BH].^[19] A strong increase is observed after several hundred minutes, reaching a relatively stable plateau later on.

As shown in **Figure 1**, the increase in both ΔN_{LD} and [BH] during dark annealing at 160 °C coincides. The maximum LeTID extent of the samples with $n = 2.05$ and $n = 2.3$ is reached

at the same time that [BH] saturates. In contrast, the maximum of ΔN_{LD} of the sample with $n = 2.19$ is reached earlier, which can be explained by an earlier onset of regeneration (compare **Figure 1a**). One distinct feature of the sample with $n = 2.19$ is its 40% higher initial τ_{eff} compared with the other two samples. While this could have an impact, the cause for the difference between the samples' onset of regeneration is yet unknown. For a clearer picture, ΔN_{LD} is plotted versus [BH] in **Figure 2**; data points obviously dominated by surface degradation are excluded here.

All samples show a similar behavior: During degradation, we observe a linear correlation between ΔN_{LD} and [BH]. In addition, the maximum of ΔN_{LD} is reached at or close to the saturation of [BH]. However, whereas ΔN_{LD} decreases afterward, we do not observe a decrease in [BH], which by contrast seems to reach a plateau (compare **Figure 1**). This behavior results in the steep drop of ΔN_{LD} at high [BH], as shown in **Figure 2**.

Please note that, as we have estimated previously,^[16] the density of *LD* ($\approx 10^{11} \text{ cm}^{-3}$) is presumably orders of magnitude lower than the detection limit of [BH] ($\approx 3 \times 10^{14} \text{ cm}^{-3}$). Therefore, a direct measurement of hydrogen-related changes caused by *LD* formation is very difficult and would always be influenced by other hydrogen-related reactions. The following implications are thus derived from observing similar kinetics.

2.1. Implications on LeTID Defect Formation

Both, the linear correlation between ΔN_{LD} and [BH] and both quantities reaching their maximum values at around the same time, are strong indications that *LD* formation and B–H pairing are limited by the same reaction. We can think of two possible explanations (see also **Figure 3**):

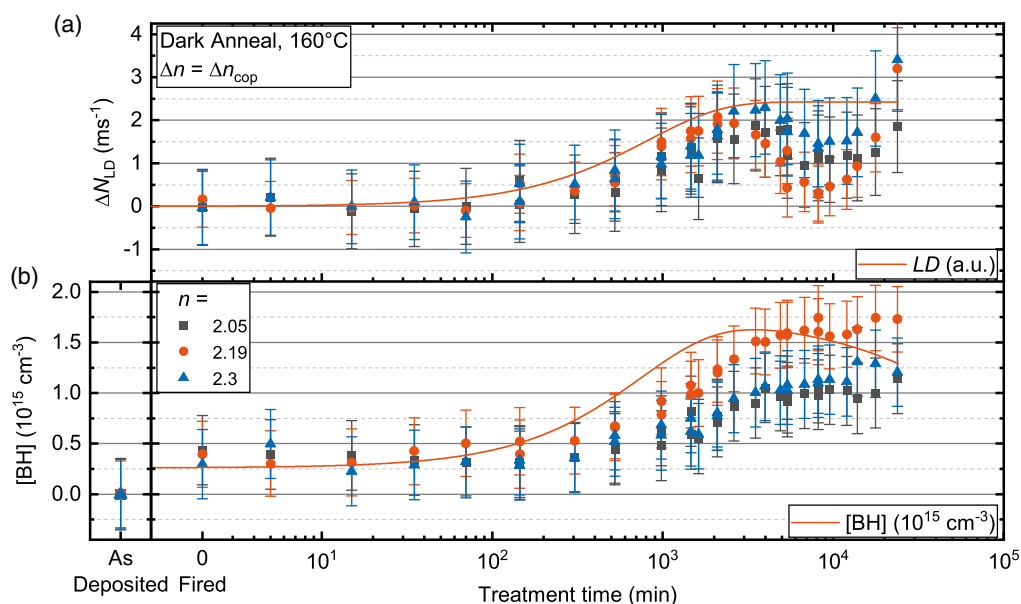


Figure 1. a,b) Evolution of LeTID defect density ΔN_{LD} (a) and BH concentration (b) according to Equation (1) and (2), respectively, during dark anneal at 160 °C. Three wafers with different refractive indices of SiN_x:H are depicted with refractive indices of $n = 2.05$ (black squares), $n = 2.19$ (red circles), and $n = 2.3$ (blue triangles). In addition, the formation of recombination-active LeTID defects *LD* (a) and B–H pairs (b) are simulated using the model described in ref. [16], depicted by the red lines. As orientation for the simulation, the [BH] values of the sample with $n = 2.19$ were used.

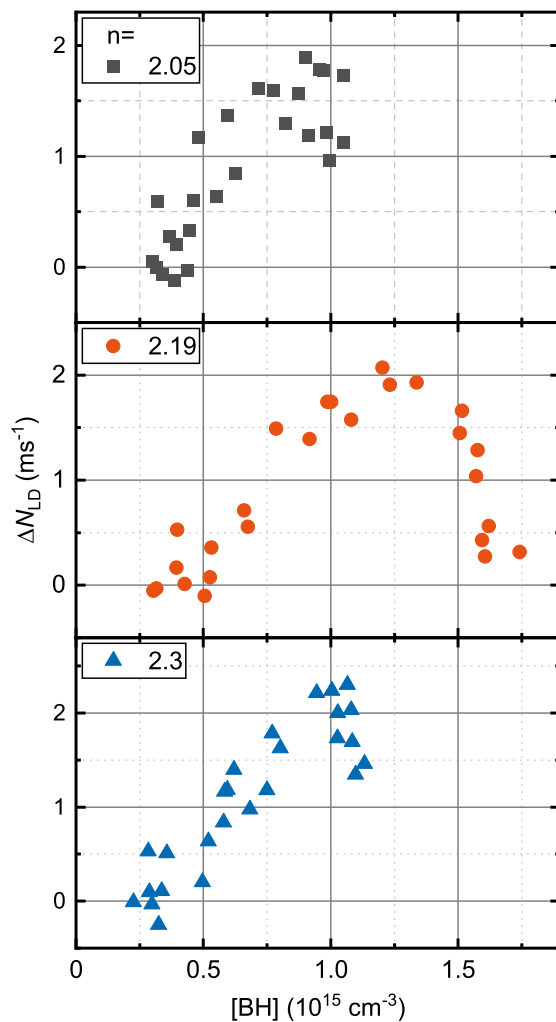


Figure 2. For every time step, the measured ΔN_{LD} below the onset of surface degradation is plotted against the B–H concentration (compare Figure 1). For reasons of presentation, error bars are omitted.

Model 1—LD Formation as an Association Process: It has been established in literature that during the treatment at 160 °C in the dark, the B–H pairs form mainly as a result of the dissociation of the hydrogen molecule H_{2A} ^[20–23] (compare Figure 3a). By analogy, it is conceivable that LD forms in parallel by an association of LP with H (Figure 3b). Both reactions would then be limited by the H_{2A} dissociation reaction. LD can be reversed into the initial state by charge carrier injection at room temperature (“temporary recovery”).^[16] In the context of model 1, the temporary recovery would mean that the LP–H complex dissociates with the dissociated hydrogen-forming H_{2A} molecules again. To the authors’ knowledge, the formation of H_{2A} during carrier injection at room temperature has not yet been observed. Although a recent report investigates the dissociation of B–H and formation of H_{2A} at 160 °C and under injection,^[24] the formation involves higher temperatures than 25 °C (compare the reverse reaction in Figure 3a). This is in accordance with previously published findings,^[20,25] where rather high temperatures were involved.

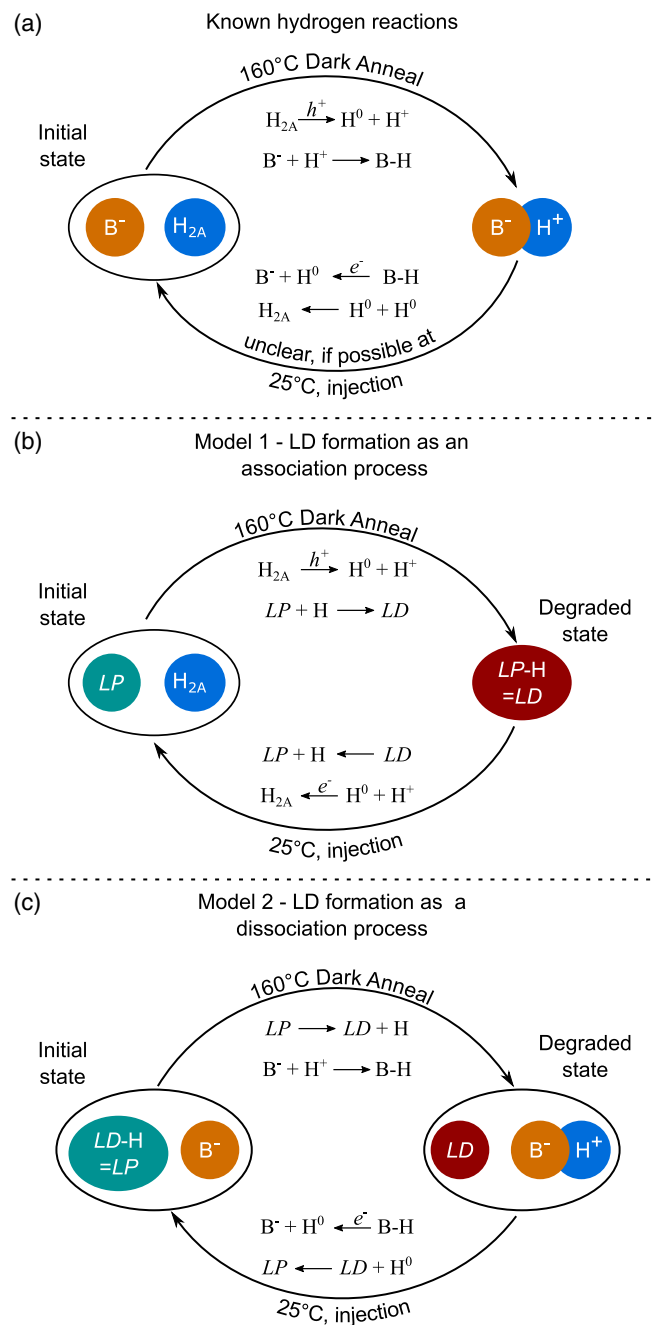


Figure 3. Schematic representation of reactions occurring during dark annealing experiments. a) Hydrogen reactions at 160 °C during dark annealing. Models 1 and 2 depict possible mechanisms of the formation of the LeTID defect LD due to the experimental results observed in this study. The reverse reactions that have to occur during temporal recovery (25 °C, charge carrier injection) are shown as well. The mechanisms involve the LeTID precursor LP, nonpassivated boron (B^-), atomic hydrogen (H , H^+ , and H^0), molecular hydrogen (H_{2A}), electrons e^- , and holes h^+ .

Model 2—LD Formation as a Dissociation Process: It is also possible that LD is formed by hydrogen dissociating from LP and binding to its sink with the remains of LP being recombination active (compare Figure 3c). In this case, boron serves as a

sink for the dissociated hydrogen and, hence, the B–H pairing is the limiting reaction.

As shown in Figure 1, [BH] reaches a saturation value. This saturation value is an equilibrium value, defined by all hydrogen reactions and influenced by parameters like the doping concentration.^[20] Following the logic of model 2, the formation of *LD* depends on the formation of B–H. This would mean that on reaching equilibrium no more changes in [BH] and ΔN_{LD} are observed. This is in accordance with the experimental observation that ΔN_{LD} reaches its maximum value at the same or similar time as [BH] saturates (compare Figure 1). As pointed out in ref. [16], this dependence on the equilibrium could also explain findings, where a lower LeTID extent was observed on wafers with lower doping concentration.^[26]

Considering the temporary recovery, B–H pairs would need to dissociate, with the dissociated hydrogen binding to *LD* to form the recombination-inactive *LP*. Even though, on a fundamental level, a complex dissociates more likely with increasing temperature, the important factor for this reverse reaction is the concentration of H^+ . To explain this, we have to consider the specifics of the B–H complex as well as the high injection dependence ($\approx \Delta n^2$) observed for temporal recovery.^[16]

It is known that the B–H complex dissociates very quickly^[27] and constant trapping/releasing of H^+ occurs.^[20] The formation and dissociation of B–H can be defined by the mass action law and its equilibrium constant K : $K = [H^+][B]/[BH]$. In addition, H^+ is subject to a further equilibrium: The fractional distributions of H^+ , H^0 , and H^- are strongly dependent on temperature and especially carrier injection.^[28] In p-type Si and at room temperature, the relative fractions of H^0 and H^- increase with increasing charge carrier injection. Therefore, by injecting charge carriers during temporal recovery, $[H^+]$ decreases and especially $[H^0]$ increases. Due to the mass action law, [BH] decreases when $[H^+]$ decreases. Thus, B–H pairs are effectively dissociated and the dissociated hydrogen is available as neutral hydrogen. In addition, it is known that H^0 is highly diffusive,^[29] thus making it the ideal candidate to associate with *LD* to form *LP*, for example, with an intermediate transition to H^+ .

Considering the current knowledge about hydrogen, we find the second mechanism—the formation of *LD* via dissociation of *LP* into H and *LD*—more likely. To substantiate this estimation, we compared the experimental evolutions of ΔN_{LD} and [BH] with numerical simulations using the model and parameters proposed in ref. [16]. The result is shown in Figure 1. Although the model predicts faster formation rates, the general trends can be well reproduced. The discrepancies indicate that further measurements are needed to fine tune the model parameters.

Please note that the current state of the model does not include specifics about the LeTID precursor, its chemical composition, its formation, and how it can be influenced. The chemical composition of *LP* correlates directly with the yet unknown chemical composition of *LD* as, according to our model, H dissociates from *LP*, resulting in the formation of *LD*. In addition, the specifics of the annihilation process of *LD* during prolonged treatment are yet unclear and thus not yet included in our model. Further investigating these open questions will lead to a thorough understanding of LeTID and might open new routes to mitigate its negative influence on silicon solar cells.

3. Conclusion

By investigating the formation of B–H pairs alongside the formation of *LD*, we have found both formations to occur at the same time. This observation indicates that both formations are limited by the same reaction, which in turn points toward two possible *LD* formation mechanisms. The first mechanism is based on an association of *LP* with H, whose source is molecular H_{2A} , whereas the second mechanism is a dissociation-based process where hydrogen dissociates from *LP*, binds to its preferred sink (in this case boron), and the remains of *LP* are recombination active. By taking the treatment conditions needed for the reverse reaction into account and combining this with the state-of-the-art knowledge of hydrogen, we consider the second mechanism a more likely process. In addition, numerical simulations based on the second mechanism reproduce the general, experimentally observed trends well. With these results as a basis, the model can be developed further toward a broader picture of LeTID by including the creation of and influences on *LP*, as well as the annihilation of *LD* on subsequent treatment.

4. Experimental Section

Sample Preparation: In this study, 4" float-zone (FZ) silicon wafers with a thickness of 250 μm and a bulk resistivity of around 0.5 Ωcm were initially cleaned via a Radio Corporation of America (RCA) cleaning sequence. An oxidation step at 1050 °C followed by a hydrofluoric acid (HF) etch was applied to negate possible bulk defects arising from the temperature budget of the deposition of passivation layer.^[30] Afterward, a POCl_3 diffusion at 900 °C was used to efficiently getter any metallic contaminants. The PSG-layer and highly doped regions at both surfaces were etched back. After another RCA sequence, the samples were passivated on both sides with 100 nm-thick $\text{SiN}_x\text{:H}$ films via plasma-enhanced chemical vapor deposition (PECVD) of different compositions: by varying the SiH_4/NH_3 gas flow, refractive indices of $n = 2.05, 2.19$, and 2.3 were achieved, aiming at different hydrogen contents in the finished samples. To activate the passivation layer and diffuse hydrogen into the bulk, the samples underwent a fast-firing process with a measured sample peak temperature of $T_{\text{sample}} = 800$ °C.

It has to be mentioned here that the deposition of $\text{SiN}_x\text{:H}$ with $n = 2.3$ was nonoptimal, resulting in an inhomogeneous $\text{SiN}_x\text{:H}$ film. However, we considered our investigation of the correlations still to be valid as the specific layer properties did not result in significant differences.

Experimental Details: To measure the effective minority charge carrier lifetime τ_{eff} , a WCT-120 device from Sinton Instruments^[31] was used. Despite our precautions, we found that the samples contained a small amount of iron. To minimize the impact of FeB pair dissociation, τ_{eff} was evaluated at the crossover point Δn_{cop} . As the resistivity changes during the dark anneal, a mean Δn_{cop} was used for each wafer to calculate the apparent defect density ΔN_{LD} at treatment time t according to

$$\Delta N_{LD} = \frac{1}{\tau_{\text{eff}}(\Delta n_{\text{cop}}, t)} - \frac{1}{\tau_{\text{eff}}(\Delta n_{\text{cop}}, t_0)} \quad (1)$$

Please note that all instabilities in carrier lifetime are reflected in this definition (compare, e.g., the study by Herguth^[32]).

At the same time as the carrier lifetime measurements, the measurement device can also be used to determine bulk resistivity, similar to the approach shown in the study by Walter et al.^[33] However, to obtain accurate resistivity measurements, the sample temperature and thickness (as pointed out by Black and Macdonald^[34]) have to be carefully taken into account. After having improved the resistivity measurement, we minimized the measurement uncertainty to 1%. As the temperature varies between measurements, the resistivity was calculated at 25 °C; from this

value, the nonpassivated boron concentration $[B^-]$ was computed. The BH pair concentration at treatment time t was then calculated from $[B^-]$ according to

$$[BH] = [B^-](t_0) - [B^-](t) \quad (2)$$

The normalization value $\tau_{\text{eff}}(\Delta n_{\text{cop}}, t_0)$ was calculated from the harmonic mean of the first five data points, where no apparent changes in τ_{eff} and $[B^-]$ were visible. For $[BH]$ calculation, the measured $[B^-]$ -value after $\text{SiN}_x\text{:H}$ deposition was used as $[B^-](t_0)$ (compare Figure 1). The initial values of $\tau_{\text{eff}}(\Delta n_{\text{cop}}, t_0)$ were $121 \mu\text{s}$ ($n = 2.05$), $179 \mu\text{s}$ ($n = 2.19$), and $128 \mu\text{s}$ ($n = 2.3$). For measurement uncertainty calculation, the uncertainty of measured τ_{eff} was estimated to 10% according to various studies.^[35,36] The uncertainty of measured resistivity was estimated to 1% according to our own reproducibility tests.

Supporting Information

Supporting Information is available from the Wiley Online Library or from the author.

Acknowledgements

This work was supported by the German Federal Ministry for Economic Affairs and Energy (BMWi) within the research projects Hydra under grants 03EE1052B and 03EE1052D and Nextstep under grant 0324171B. B.H. thanks “Nagelschneider Stiftung” for funding his dissertation project. The authors are responsible for the content.

Open access funding enabled and organized by Projekt DEAL.

Conflict of Interest

The authors declare no conflict of interest.

Data Availability Statement

Research data are not shared.

Keywords

boron, defects, hydrogen, light- and elevated-temperature-induced degradations, silicon

Received: December 15, 2020
Revised: February 26, 2021
Published online: April 4, 2021

- [1] S. J. Pearton, J. W. Corbett, T. S. Shi, *Appl. Phys. A* **1987**, 43, 153.
- [2] S. Wilking, A. Herguth, G. Hahn, *J. Appl. Phys.* **2013**, 113, 194503.
- [3] K. Ramspeck, S. Zimmermann, H. Nagel, A. Metz, Y. Gassenbauer, B. Birkmann, A. Seidl, *27th Eur. Photovoltaics Sol. Energy Conf. Exhib.* **2012**, 1, 861.
- [4] F. Kersten, P. Engelhart, H.-C. Ploigt, A. Stekolnikov, T. Lindner, F. Stenzel, M. Bartzsch, A. Szpeth, K. Petter, J. Heitmann, J. W. Müller, *Sol. Energy Mater. Sol. Cells* **2015**, 142, 83.
- [5] D. Chen, M. Kim, B. V. Stefani, B. J. Hallam, M. D. Abbott, C. E. Chan, R. Chen, D. N. Payne, N. Nampalli, A. Ciesla, T. H. Fung, K. Kim, S. R. Wenham, *Sol. Energy Mater. Sol. Cells* **2017**, 172, 293.
- [6] T. Niewelt, M. Selinger, N. E. Grant, W. Kwapil, J. D. Murphy, M. C. Schubert, *J. Appl. Phys.* **2017**, 121, 185702.
- [7] D. Sperber, A. Heilemann, A. Herguth, G. Hahn, *IEEE J. Photovoltaics* **2017**, 7, 463.
- [8] C. Chan, T. H. Fung, M. Abbott, D. Payne, A. Wenham, B. Hallam, R. Chen, S. Wenham, *Sol. RRL* **2017**, 1, 1600028.
- [9] T. H. Fung, M. Kim, D. Chen, C. E. Chan, B. J. Hallam, R. Chen, D. N. Payne, A. Ciesla, S. R. Wenham, M. D. Abbott, *Sol. Energy Mater. Sol. Cells* **2018**, 184, 48.
- [10] P. Hamer, B. Hallam, R. S. Bonilla, P. P. Altermatt, P. Wilshaw, S. Wenham, *J. Appl. Phys.* **2018**, 123, 43108.
- [11] U. Varshney, M. Kim, M. U. Khan, P. Hamer, C. Chan, M. Abbott, B. Hoex, *IEEE J. Photovoltaics* **2021**, 11, 65.
- [12] T. H. Fung, M. Kim, D. Chen, A. Samadi, C. E. Chan, B. J. Hallam, S. Wenham, M. Abbott, *AIP Conf. Proc.* **2018**, 1999, 130004.
- [13] D. Chen, P. Hamer, M. Kim, C. Chan, A. Ciesla nee Wenham, F. Rougieux, Y. Zhang, M. Abbott, B. Hallam, *Sol. Energy Mater. Sol. Cells* **2020**, 207, 110353.
- [14] J. Schmidt, D. Bredemeier, D. C. Walter, *IEEE J. Photovoltaics* **2019**, 9, 1497.
- [15] D. Chen, *Ph.D. Thesis*, University of New South Wales, Sydney, Australia **2020**.
- [16] W. Kwapil, J. Schon, T. Niewelt, M. C. Schubert, *IEEE J. Photovoltaics* **2020**, 10, 1591.
- [17] D. Bredemeier, D. C. Walter, R. Heller, J. Schmidt, *36th Eur. Photovoltaics Sol. Energy Conf. Exhib.* **2019**, 1, 112.
- [18] D. Sperber, A. Graf, D. Skorka, A. Herguth, G. Hahn, *IEEE J. Photovoltaics* **2017**, 7, 1627.
- [19] M. J. Binns, R. C. Newman, S. A. McQuaid, E. C. Lightowers, *Mater. Sci. Forum* **1993**, 143–147, 861.
- [20] V. V. Voronkov, R. Falster, *Phys. Status Solidi B* **2017**, 254, 1600779.
- [21] A. Leitch, T. Zundel, T. Prescha, J. Weber, *Mater. Sci. Forum* **1992**, 83–87, 21.
- [22] N. M. Johnson, C. Doland, F. Ponce, J. Walker, G. Anderson, *Phys. B* **1991**, 170, 3.
- [23] T. Zundel, J. Weber, *Phys. Rev. B* **1991**, 43, 4361.
- [24] D. C. Walter, D. Bredemeier, R. Falster, J. Schmidt, V. V. Voronkov, *37th Eur. Photovoltaics Sol. Energy Conf. Exhib.* **2020**, 1, 140.
- [25] R. E. Pritchard, J. H. Tucker, R. C. Newman, E. C. Lightowers, *Semicond. Sci. Technol.* **1999**, 14, 77.
- [26] B. Hammann, J. Engelhardt, D. Sperber, A. Herguth, G. Hahn, *IEEE J. Photovoltaics* **2020**, 10, 85.
- [27] T. Zundel, J. Weber, *Phys. Rev. B* **1989**, 39, 13549.
- [28] C. Sun, F. E. Rougieux, D. Macdonald, *J. Appl. Phys.* **2015**, 117, 45702.
- [29] P. Hamer, B. Hallam, S. Wenham, M. Abbott, *IEEE J. Photovoltaics* **2014**, 4, 1252.
- [30] N. E. Grant, V. P. Markevich, J. Mullins, A. R. Peaker, F. Rougieux, D. Macdonald, *Phys. Status Solidi RRL* **2016**, 10, 443.
- [31] R. A. Sinton, A. Cuevas, *Appl. Phys. Lett.* **1996**, 69, 2510.
- [32] A. Herguth, *IEEE J. Photovoltaics* **2019**, 9, 1182.
- [33] D. C. Walter, D. Bredemeier, R. Falster, V. V. Voronkov, J. Schmidt, *Sol. Energy Mater. Sol. Cells* **2019**, 200, 109970.
- [34] L. E. Black, D. H. Macdonald, *IEEE J. Photovoltaics* **2019**, 9, 1563.
- [35] A. L. Blum, J. S. Swirhun, R. A. Sinton, F. Yan, S. Herasimenka, T. Roth, K. Lauer, J. Haunschild, B. Lim, K. Bothe, Z. Hameiri, B. Seipel, R. Xiong, M. Dhamrin, J. D. Murphy, *IEEE J. Photovoltaics* **2014**, 4, 525.
- [36] K. R. McIntosh, R. A. Sinton, *23rd Eur. Photovoltaics Sol. Energy Conf. Exhib.* **2008**, 1, 77.